

Variational Multiple Gaussian Approximation for Time-dependent Solutions of Langevin Equations

Yoshihiko Hasegawa*

*Department of Information and Communication Engineering,
Graduate School of Information Science and Technology,
The University of Tokyo, Tokyo 113-8656, Japan*

(Dated: May 16, 2022)

Abstract

We propose a variational multiple Gaussian approximation (VMGA) for dynamical solutions of Langevin equations, determining time-dependent parameters of superposed Gaussian distributions by the variational principle. We apply the proposed VMGA to systems driven by a chaotic signal, where the conventional Fourier method cannot be adopted, and calculate the time evolution of probability density functions (PDFs) and moments. Both white and colored Gaussian noises are included for the fluctuation. Our calculations show that time-dependent PDFs obtained by VMGA agree excellently with those obtained by Monte Carlo simulations. The correlation between the chaotic input signal and the mean are also calculated as a function of the noise intensity, which confirms the occurrence of aperiodic stochastic resonance with both white and colored noises.

PACS numbers: 02.60.-x, 05.10.Gg

*Corresponding author : yoshihiko.hasegawa@gmail.com

I. INTRODUCTION

Langevin equations can model systems subject to fluctuations and hence have many applications in diverse research fields such as physics, chemistry, financial engineering, and biology [1–3]. Without a driving force, systems subject to white Gaussian noise relax to their stationary states. For one-dimensional stationary systems, the probability density function (PDF) can be obtained in a closed form for many cases. However, in the presence of a driving force, its time-dependent solution is rarely available even for one-dimensional systems. Recent advancements in nonequilibrium theory [4, 5] strongly demand reliable methods for time-dependent solutions of Langevin equations for systems driven by time-dependent external forces. The moment method (MM) is widely used to study dynamics [6–8]; it considers the time evolution of moments of PDFs [in most cases, up to the second-order moments (mean and variance) are considered]. If we truncate at the second moment (i.e., n th-order terms where $n \geq 3$ are ignored), the number of differential equations is $N(N + 3)/2$, where N is the dimensionality of the model; thus, with current computer capabilities, the MM is tractable up to $N \sim 10$. Although the MM can provide satisfactory results for linear (or weakly nonlinear) systems, its applicability collapses even for simple bistable models. Here, for time-dependent solutions of Langevin models, we propose an approximation technique in which PDFs are represented by superposed multiple Gaussian distributions, obtaining time-evolution equations for parameters of each of the Gaussian distributions with the variational principle. We call the proposed method the variational multiple Gaussian approximation (VMGA). Gaussian approximations have a long history in quantum mechanics. Heller introduced the Gaussian wavepacket method, which approximates time-dependent solutions of Schrödinger equations with a Gaussian packet by obtaining equations for the mean and variance through the McLachlan variational principle [9] (other equivalent variational principles are also known [10–12]). Several researchers extended Heller’s approach to incorporate multiple Gaussian distributions [13–15], and these methods can provide reliable solutions for time-dependent wave functions by virtue of their multiplicity. Although the effectiveness of the multiple Gaussian method with the McLachlan variational principle has been shown to approximate wave functions in quantum mechanics [13–15], its capability has not been shown in the context of time-dependent Fokker-Planck equations (FPEs).

Similar approaches to Langevin equations were developed with the Kalman filter [16] by

Terejanu *et al.*, who proposed an approximation scheme based on multiple Gaussian distributions. They calculated the mean and variance of each distribution, using the extended Kalman filter with a fixed weight. After calculating the mean and variance, they optimized the weight, using quadratic programming to minimize the squared error. Their method requires quadratic programming, and the time evolution of the mean follows deterministic dynamics [i.e., $\dot{\boldsymbol{\mu}} = \mathbf{f}(\boldsymbol{\mu})$, where $\boldsymbol{\mu}$ is a vector of the means of each of the Gaussian distributions and \mathbf{f} is a drift term], which is not necessarily optimal. Instead, we directly calculate the mean, variance, and weight in a unified way that does not require ad hoc mathematical programming. Furthermore, as the McLachlan variational principle is minimized with respect to the squared error, our method always yields an (near) optimal time evolution of the mean, variance, and weight. There are several numerical approaches to the study of the dynamics of FPEs that represent PDFs by using complete set functions (e.g., a matrix continued-fraction method; for details, see Ref. [17] and the references therein). More-direct numerical schemes, such as a finite-element method [18, 19] and a finite-difference method [20], have also been studied. These approaches, however, have high computational costs.

To investigate the effectiveness of VMGA, we applied it to a quartic bistable system subject to white or colored noise. Although a bistable system can describe switching dynamics and has many and varied applications to realistic problems [21], its nonlinearity makes the application of the simple MM difficult. We consider a system driven by a chaotic signal (the Rössler oscillator). When the signal is aperiodic, we cannot use a Fourier series expansion, as is often employed for periodic cases [22], and hence many studies have resorted to using direct Monte Carlo (MC) simulations. We show that VMGA can accurately approximate the time-dependent moments and the PDFs of the systems for both white (one-dimensional) and colored (two-dimensional) noises. Calculating the correlation between the chaotic input signal and the mean of the dynamics [cf. Eq. (26)], we show that the correlation is maximal when the noise is of intermediate strength; this is a signature of aperiodic stochastic resonance (ASR) [23, 24] [for general stochastic resonance (SR), see [25–29] and the references therein]. Furthermore, from the results with colored noise, we show that the time correlation weakens the magnitude of the ASR.

The remainder of this paper is organized as follows. In Section II, we introduce our proposed method, the VMGA, and provide a detailed explanation of the McLachlan variational principle for FPEs. We obtain implicit differential equations that should be satisfied by

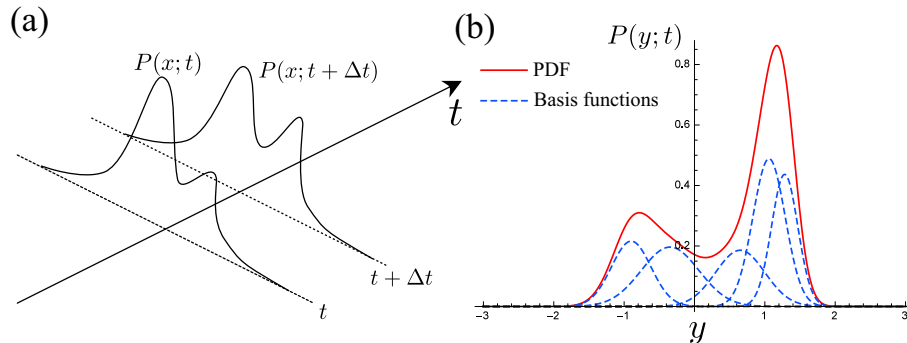


FIG. 1: (Color online) (a) Illustration of time evolution of a PDF. If the PDF at time t [i.e., $P(x; t)$] is known, the optimal $P(x; t + \Delta t)$ is given by $P(x; t + \Delta t) \simeq P(x; t) + \Delta t \Theta(x; t)$, where $\Theta(x; t)$ is optimal. (b) Example of an approximative PDF (solid line) that is a superposition of five Gaussian distributions (dashed line).

the mean, variance, and weights of each of the Gaussian distributions. In Section III, we investigate the effectiveness of VMGA by applying it to two cases: a bistable system driven by a chaotic signal subject to (a) white noise, and (b) colored noise. Finally, we provide a discussion and present our conclusions in Section IV.

II. METHODS

We consider an N -dimensional Langevin equation (the Stratonovich interpretation)

$$\frac{dx_i}{dt} = f_i(\mathbf{x}, t) + \sum_{j=1}^{N_g} g_{ij}(\mathbf{x}, t) \xi_j(t), \quad (i = 1, 2, \dots, N), \quad (1)$$

where $\mathbf{x} = (x_1, \dots, x_N)^\top$ (\top denotes the transpose operation) is an N -dimensional column vector, $f_i(\mathbf{x}, t)$ and $g_{ij}(\mathbf{x}, t)$ denote i th drift and multiplicative terms, respectively, $\xi_i(t)$ is white Gaussian noise with the correlation $\langle \xi_i(t) \xi_j(t') \rangle = 2\delta_{ij} \delta(t - t')$, and N_g is the number of noise sources [17]. The Langevin equation (1) has the corresponding FPE [17]

$$\frac{\partial}{\partial t} P(\mathbf{x}; t) = \hat{L}(\mathbf{x}, t) P(\mathbf{x}; t), \quad (2)$$

where $P(\mathbf{x}; t)$ is the probability density of \mathbf{x} at time t , and $\hat{L}(\mathbf{x}, t)$ is an FPE operator defined by

$$\hat{L}(\mathbf{x}, t) = - \sum_i \frac{\partial}{\partial x_i} F_i(\mathbf{x}, t) + \sum_{i,j} \frac{\partial^2}{\partial x_i \partial x_j} G_{ij}(\mathbf{x}, t). \quad (3)$$

Here $F_i(\mathbf{x}, t) = f_i(\mathbf{x}, t) + \sum_{k,j} g_{kj}(\mathbf{x}, t) \partial_{x_k} g_{ij}(\mathbf{x}, t)$ and $G_{ij}(\mathbf{x}, t) = \sum_k g_{ik}(\mathbf{x}, t) g_{jk}(\mathbf{x}, t)$ (note that the VMGA can be applied to the Itô interpretation by modifying $F_i(\mathbf{x}, t)$) [17]. We are interested in a time-dependent solution $P(\mathbf{x}; t)$ of Eq. (2). We approximate the time evolution by using the McLachlan variational principle (similar variational principles are known in other fields), which is explained below for the FPE.

Let $\Theta(\mathbf{x}; t)$ be the time derivative of $P(\mathbf{x}; t)$, i.e., $\Theta(\mathbf{x}; t) = \dot{P}(\mathbf{x}; t)$. We focus on a specific time t , where $P(\mathbf{x}; t)$ is already known, and we want to know the optimal time evolution $\Theta(\mathbf{x}; t)$ [Fig. 1(a)]. In other words, we want to calculate $P(\mathbf{x}; t + \Delta t)$, where Δt is a sufficiently small increment, from a known $P(\mathbf{x}; t)$ by using $P(\mathbf{x}; t + \Delta t) \simeq P(\mathbf{x}; t) + \Delta t \Theta(\mathbf{x}; t)$. From Eq. (2), the optimal $\Theta(\mathbf{x}; t)$ should minimize

$$R[\Theta] = \int_{-\infty}^{\infty} \left\{ \hat{L}(\mathbf{x}, t) P(\mathbf{x}; t) - \Theta(\mathbf{x}; t) \right\}^2 d\mathbf{x}, \quad (4)$$

where we have abbreviated as follows: $\int_{-\infty}^{\infty} dx_1 \cdots \int_{-\infty}^{\infty} dx_n = \int_{-\infty}^{\infty} d\mathbf{x}$. Although we may obtain the optimal $P(\mathbf{x}; t + \Delta t)$ by solving Eq. (4) with respect to Θ , the optimal Θ does not necessarily yield solutions that satisfy the normalization condition $\int_{-\infty}^{\infty} P(\mathbf{x}; t) d\mathbf{x} = 1$ at any time t . Therefore we should impose an additional constraint on Eq. (4). When $P(\mathbf{x}; t)$ is normalized at $t = 0$, then the normalization of $P(\mathbf{x}; t)$ at $t > 0$ is satisfied by the equation given by

$$\frac{d}{dt} \int_{-\infty}^{\infty} P(\mathbf{x}; t) d\mathbf{x} = \int_{-\infty}^{\infty} \Theta(\mathbf{x}; t) d\mathbf{x} = 0. \quad (5)$$

Therefore, to minimize Eq. (4) with the normalization condition of Eq. (5), we have to optimize the following equation:

$$\tilde{R}[\Theta] = \int_{-\infty}^{\infty} \left\{ \hat{L}(\mathbf{x}, t) P(\mathbf{x}; t) - \Theta(\mathbf{x}; t) \right\}^2 d\mathbf{x} + \lambda \int_{-\infty}^{\infty} \Theta(\mathbf{x}; t) d\mathbf{x}, \quad (6)$$

where λ is the Lagrange multiplier. With a variation of $\delta\Theta(\mathbf{x}; t)$ in Eq. (6), $\delta\tilde{R} = \tilde{R}[\Theta + \delta\Theta] - \tilde{R}[\Theta]$ should vanish for the optimal $\Theta(\mathbf{x}; t)$, yielding

$$\int_{-\infty}^{\infty} \delta\Theta \left\{ \hat{L}(\mathbf{x}, t) P(\mathbf{x}; t) - \Theta(\mathbf{x}; t) + \lambda \right\} d\mathbf{x} = 0, \quad (7)$$

where we redefined λ for notational convenience. Suppose $P(\mathbf{x}; t)$ is a function parametrized by time-dependent K values $\boldsymbol{\theta}(t) = (\theta_1(t), \theta_2(t), \dots, \theta_K(t))$:

$$P(\mathbf{x}; t) = P(\mathbf{x}; \boldsymbol{\theta}(t)), \quad (8)$$

where the time-dependence of $P(\mathbf{x}; t)$ is represented through $\boldsymbol{\theta}(t)$. Thus $\Theta(\mathbf{x}; t)$ is given by

$$\Theta(\mathbf{x}; t) = \Theta(\mathbf{x}; \boldsymbol{\theta}(t), \dot{\boldsymbol{\theta}}(t)). \quad (9)$$

The variation $\delta\Theta$ can be achieved only through the variation of $\dot{\boldsymbol{\theta}}$ ($\boldsymbol{\theta}$ cannot be changed, as we assumed that $P(\mathbf{x}; t) = P(\mathbf{x}; \boldsymbol{\theta}(t))$ is fixed at time t):

$$\delta\Theta = \sum_{\ell=1}^K \frac{\partial\Theta(\mathbf{x}; \boldsymbol{\theta}, \dot{\boldsymbol{\theta}})}{\partial\dot{\theta}_\ell} \delta\dot{\theta}_\ell, \quad (10)$$

where

$$\begin{aligned} \frac{\partial\Theta(\mathbf{x}; \boldsymbol{\theta}, \dot{\boldsymbol{\theta}})}{\partial\dot{\theta}_\ell} &= \frac{\partial}{\partial\dot{\theta}_\ell} \frac{dP(\mathbf{x}; \boldsymbol{\theta})}{dt}, \\ &= \frac{\partial}{\partial\dot{\theta}_\ell} \left(\sum_{\ell'=1}^K \frac{\partial P(\mathbf{x}; \boldsymbol{\theta})}{\partial\theta_{\ell'}} \dot{\theta}_{\ell'} \right), \\ &= \frac{\partial P(\mathbf{x}; \boldsymbol{\theta})}{\partial\theta_\ell}. \end{aligned} \quad (11)$$

For the variation $\delta\dot{\boldsymbol{\theta}} = (\delta\dot{\theta}_1, \dots, \delta\dot{\theta}_K)$, we consider the simplest orthogonal case:

$$\delta\dot{\boldsymbol{\theta}} = (1, 0, 0, \dots, 0), (0, 1, 0, \dots, 0), \dots, (0, 0, 0, \dots, 1).$$

Substituting Eqs. (10) and (11) into Eq. (7), we have K constraints

$$\int_{-\infty}^{\infty} \frac{\partial P(\mathbf{x}; \boldsymbol{\theta})}{\partial\theta_\ell} \left\{ \hat{L}(\mathbf{x}, t) P(\mathbf{x}; \boldsymbol{\theta}) - \Theta(\mathbf{x}; \boldsymbol{\theta}, \dot{\boldsymbol{\theta}}) + \lambda \right\} d\mathbf{x} = 0 \quad (\ell = 1, 2, \dots, K), \quad (12)$$

which is the variational principle for FPEs that is equivalent to the McLachlan one. The Lagrange multiplier λ should be determined by Eq. (5).

We next show an explicit form of $P(\mathbf{x}; \boldsymbol{\theta}(t))$. We approximate $P(\mathbf{x}; t)$ with a superposition of multiple Gaussian distributions (Fig. 1(b)):

$$P(\mathbf{x}; \boldsymbol{\theta}(t)) = \sum_{m=1}^{N_B} r_m g(\mathbf{x}; \mathbf{A}_m, \mathbf{b}_m), \quad (13)$$

where $g(\mathbf{x}; \mathbf{A}, \mathbf{b})$ is an unnormalized Gaussian distribution:

$$g(\mathbf{x}; \mathbf{A}, \mathbf{b}) = \exp(-\mathbf{x}^\top \mathbf{A} \mathbf{x} + \mathbf{b}^\top \mathbf{x}). \quad (14)$$

Here \mathbf{A} is an $N \times N$ symmetric matrix (positive definite), \mathbf{b} is an N -dimensional column vector, r_m is a parameter that combines the weight of the m th Gaussian with a normalization

constant, and N_B is the number of basis functions. We employed a parametrization of Eq. (14) that is different from the conventional multivariate Gaussian representation, because multidimensional calculations are easier with Eq. (14) (cf. Appendix A). For instance, multiplication is simply given by

$$g(\mathbf{x}; \mathbf{A}_m, \mathbf{b}_m)g(\mathbf{x}; \mathbf{A}_{m'}, \mathbf{b}_{m'}) = g(\mathbf{x}; \mathbf{A}_m + \mathbf{A}_{m'}, \mathbf{b}_m + \mathbf{b}_{m'}).$$

We optimized all of the Gaussian parameters by using the variational principle, i.e., $\boldsymbol{\theta} = (\mathbf{A}_m, \mathbf{b}_m, r_m)_{m=1}^{N_B}$. For an N -dimensional system and N_B basis functions, the total number of parameters is

$$K = \frac{N_B(N+1)(N+2)}{2}. \quad (15)$$

From Eq. (12) and the constraint of Eq. (5), we obtain $(K+1)$ implicit differential equations of the following form:

$$H_\ell(\boldsymbol{\theta}(t), \dot{\boldsymbol{\theta}}(t), \lambda(t)) = 0, \quad \ell = 1, 2, \dots, K, K+1. \quad (16)$$

Equation (16) is called a differential algebraic equation (DAE) [30], which can be solved numerically by using *MATHEMATICA* 10 (NDSolve function). VMGA does not accept arbitrary initial values, because $(\mathbf{A}_m, \mathbf{b}_m, r_m)_{m=1}^{N_B}$ should satisfy the normalizing condition, which can be obtained from Eqs. (A3)–(A5) (cf. Appendix B).

III. RESULTS

We applied the VMGA to two double-well systems driven by chaotic signals, one subject to white Gaussian noise (Section III A) and the other subject to colored Gaussian noise (Section III B). We also performed MC simulations to show the reliability of the VMGA.

A. Chaotically-driven bistable potential subject to white noise

We applied the VMGA to a driven bistable potential subject to white Gaussian noise. Specifically, we applied it to a one-dimensional potential driven by an input signal $I(t)$:

$$\frac{dy}{dt} = y - y^3 + I(t) + \sqrt{D}\xi(t), \quad (17)$$

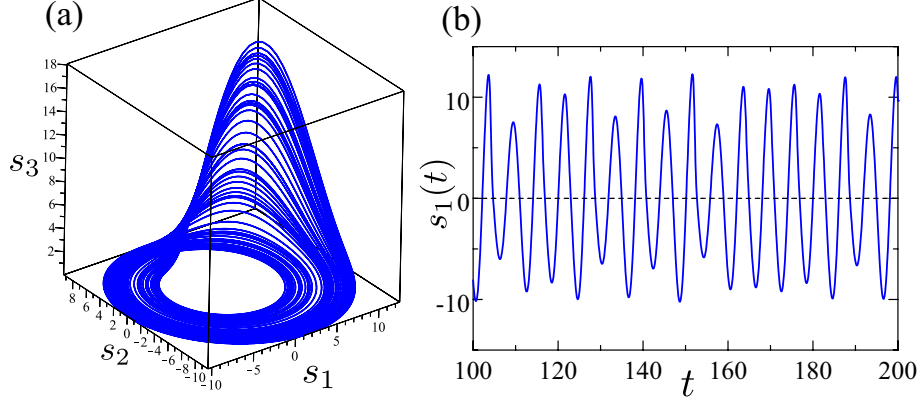


FIG. 2: (Color online) Trajectories of Rössler chaos [Eqs. (19)–(21)]: (a) 3D plot of s_1 , s_2 , and s_3 ; and (b) s_1 as a function of t . The parameters are $c_1 = 0.15$, $c_2 = 0.2$ and $c_3 = 7.1$.

where D is the noise intensity and $\xi(t)$ is white Gaussian noise with the correlation $\langle \xi(t)\xi(t') \rangle = 2\delta(t - t')$. The FPE operator $\hat{L}(\mathbf{x}, t) = \hat{L}(y, t)$ is given by

$$\hat{L}(y, t) = -\frac{\partial}{\partial y} \{y - y^3 + I(t)\} + D \frac{\partial^2}{\partial y^2}. \quad (18)$$

Substituting Eq. (18) into Eq. (12), we can calculate K coupled DAEs with respect to $\boldsymbol{\theta} = (\mathbf{A}_m, \mathbf{b}_m, r_m)_{m=1}^{N_B}$ (for the one-dimensional case, $\mathbf{A}_m = a_m$ and $\mathbf{b}_m = b_m$, where a_m, b_m are real scalar quantities) requiring moments of the Gaussian distribution of up to the sixth order ($\int_{-\infty}^{\infty} y^{n_y} g(y; \mathbf{A}, \mathbf{b}) dy$, with $n_y \leq 6$). For the input signal $I(t)$, we used the Rössler oscillator [31]:

$$\frac{ds_1}{dt} = -s_2 - s_3, \quad (19)$$

$$\frac{ds_2}{dt} = s_1 + c_1 s_2, \quad (20)$$

$$\frac{ds_3}{dt} = c_2 + s_3(s_1 - c_3). \quad (21)$$

Here, c_i are parameters of the oscillator, and we used $c_1 = 0.15$, $c_2 = 0.2$, and $c_3 = 7.1$ (identical to the values used in Ref. [32]), with which Eqs. (19)–(21) exhibit chaotic dynamics. Figures 2(a) and (b) show trajectories of the Rössler oscillator for (a) s_1 , s_2 , and s_3 , and (b) s_1 as a function of time t . The average peak-to-peak interval (which corresponds to the period of the oscillations) of $s_1(t)$ is about 6. We define the input signal as

$$I(t) = \alpha s_1(\omega t), \quad (22)$$

where α is the input strength and ω is the reciprocal of the time-scale (this corresponds to the angular frequency of the periodic oscillations). Although time-dependent solutions of

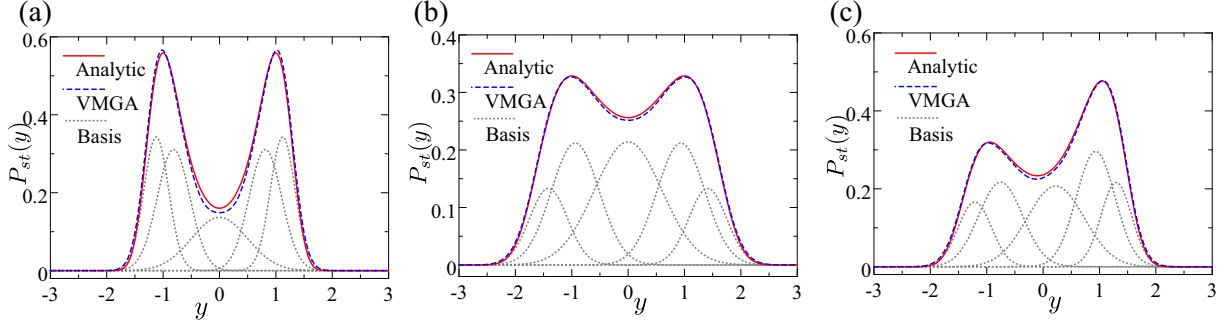


FIG. 3: (Color online) Stationary PDFs $P_{st}(y)$ obtained by analytic calculation of Eq. (25) (solid line) and by the VMGA with $N_B = 5$ (dashed line) for (a) $D = 0.2$ and $\kappa = 0$, (b) $D = 1.0$ and $\kappa = 0$, and (c) $D = 0.5$ and $\kappa = 0.1$. In (a)–(c), the dot-dashed lines denote each of the single bases of the VMGA.

periodically driven systems are often represented as a Fourier series expansion [22], such an expansion cannot be used for a chaotically driven system.

The Lagrange multiplier λ in Eq. (7) should be determined by the normalization constraint of Eq. (5). For the one-dimensional case, the constraint is

$$\frac{d}{dt} \int_{-\infty}^{\infty} P(\mathbf{x}; \boldsymbol{\theta}(t)) d\mathbf{x} = \frac{d}{dt} \int_{-\infty}^{\infty} \sum_{m=1}^{N_B} r_m(t) \exp(-a_m(t)y^2 + b_m(t)y) dy = 0, \quad (23)$$

yielding

$$0 = \sum_{m=1}^{N_B} \frac{\sqrt{\pi}}{4a_m(t)^{5/2}} \left[4a_m(t)^2 \dot{r}_m(t) - 2a_m(t)r_m(t) \left\{ \dot{a}_m(t) - b_m(t)\dot{b}_m(t) \right\} - b_m(t)^2 \dot{a}_m(t)r_m(t) \right] \exp\left(\frac{b_m(t)^2}{4a_m(t)}\right). \quad (24)$$

Equation (24) should be solved along with the DAEs obtained from Eq. (7); the total dimensionality of the DAEs is $K + 1$.

We first study a stationary case (i.e., $I(t) = \kappa$, where κ is a constant parameter), because stationary PDFs can be obtained analytically for a quartic potential. Note that the VMGA in a stationary case is equivalent to that given in Ref. [33]. A stationary PDF is given by

$$P_{st}(y) = \frac{1}{Z(D)} \exp\left[-\frac{U(y)}{D}\right], \quad (25)$$

where $Z(D) = \int_{-\infty}^{\infty} \exp(-U(y)/D) dy$ (numerically integrated) and $U(x)$ is a potential function $U(y) = -\int (y - y^3 + \kappa) dy = y^4/4 - y^2/2 - \kappa y$. The stationary PDF of a VMGA is

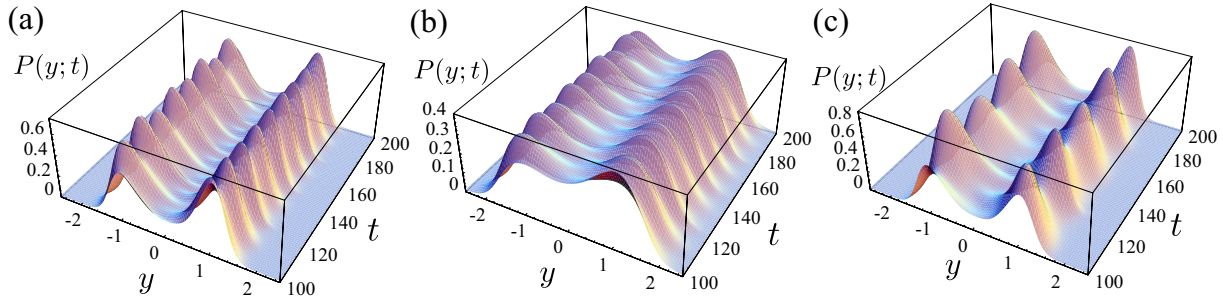


FIG. 4: (Color online) Dynamical PDFs $P(y;t)$ as functions of y and t obtained by the VMGA with $N_B = 5$ for (a) $D = 0.2$, $\alpha = 0.02$ and $\omega = 0.5$; (b) $D = 1.0$, $\alpha = 0.02$ and $\omega = 0.5$; and (c) $D = 0.2$, $\alpha = 0.02$ and $\omega = 0.25$.

obtained by letting the system evolve for a long enough time that it equilibrates. Although in the VMGA, calculations with larger N_B can yield more accurate results, we employed $N_B = 5$ (total parameter size is $K = 15$ [Eq. (15)]) because numerical instability occurs for excessively large N_B due to the nonorthogonality of multiple Gaussian distributions. Figure 3 shows the stationary distributions of the VMGA ($N_B = 5$; solid line) and the analytic solutions obtained for Eq. (25) (dashed line) for (a) $D = 0.2$ and $\kappa = 0$; (b) $D = 1.0$ and $\kappa = 0$; and (c) $D = 0.5$ and $\kappa = 0.1$. In all parameter settings, the VMGA shows very good agreement with the analytical solutions, including the asymmetric case [Fig. 3(c)]. In Fig. 3(a)–(c), the dot-dashed lines denote the Gaussian bases constituting the PDFs of the VMGA; we can see that the two bases form one well (and four bases will form two wells) and the other well is located at the center of the PDFs. From the positions of the bases, we see that the means of Gaussian bases are not positioned at the bottom of the well; this indicates that the means of the Gaussians do not follow deterministic dynamics.

We next studied the dynamical case, where the input $I(t)$ is given by Eq. (22). Figure 4 displays the $P(y;t)$ as functions of y and t , which are calculated by the VMGA with $N_B = 5$, for (a) $D = 0.2$, $\alpha = 0.02$ and $\omega = 0.5$; (b) $D = 1.0$, $\alpha = 0.02$ and $\omega = 0.5$; and (c) $D = 0.2$, $\alpha = 0.02$ and $\omega = 0.25$. To verify the $P(y;t)$ calculated by the VMGA, we evaluated the accuracy of the PDFs $P(y;t)$ at time $t = 100$ by calculating the VMGA and by performing MC simulations (we selected $t = 100$ so that we could ignore the effects of the initial values). For the MC simulations, the PDFs were constructed by repeating the stochastic simulations 20000 times (time resolution is 0.0001). Figures 5(a)–(c) show the PDFs calculated by the MC simulations (circles), the VMGA (dashed line), and each of the bases of the VMGA

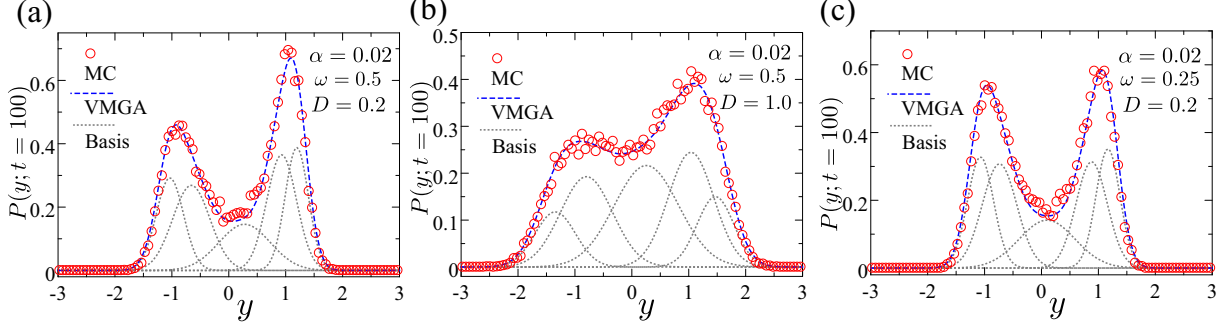


FIG. 5: (Color online) PDFs $P(y; t)$ at time $t = 100$ obtained by MC simulations (circles), the VMGA with $N_B = 5$ (dashed line), and each of the Gaussian bases of the VMGA (dotted line); the parameters in panels (a)–(c) are the same as in Figs. 4(a)–(c), respectively.

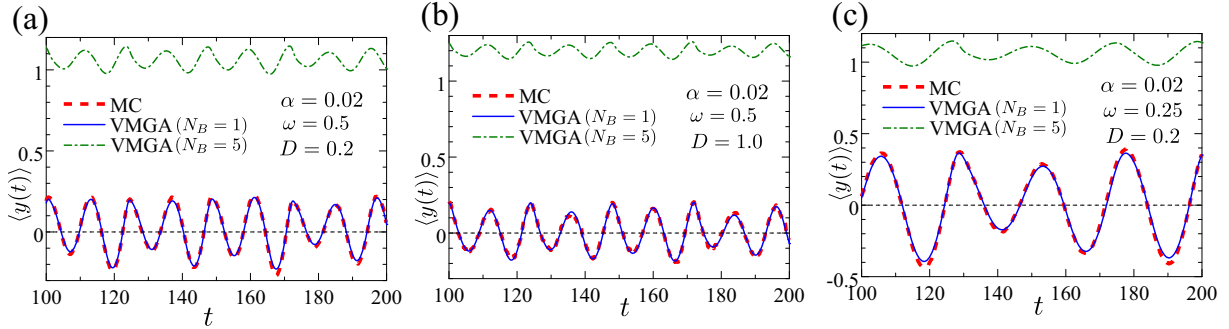


FIG. 6: (Color online) Mean $\langle y(t) \rangle$ as a function of t as obtained by MC simulations (dashed line), the VMGA with $N_B = 5$ (solid line), and the VMGA with $N_B = 1$ (dot-dashed line); the parameters in panels (a)–(c) are the same as in Figs. 4(a)–(c), respectively.

(dotted line). The parameter settings for panels (a), (b), and (c) correspond to those in Figs. 4(a), (b), and (c), respectively. For all parameter settings, the PDFs of the VMGA are in excellent agreement with those obtained by the MC simulations; this verifies the reliability of the VMGA with respect to the PDFs at a specified time.

In order to see the dynamical aspects of the VMGA, we also compared the mean $\langle y(t) \rangle$ obtained by the MC simulations to that obtained by the VMGA for the interval $t = 100–200$ (we did not consider the interval $t = 0–100$ because of the initial value effects). In Figs. 6(a)–(c), we show the mean $\langle y(t) \rangle$ calculated by the MC simulations (dashed line), the VMGA with $N_B = 5$ (solid line), and the VMGA with $N_B = 1$ (dot-dashed line). The parameter settings for (a), (b), and (c) correspond to those used in Figs. 4(a), (b), and (c), respectively. For the MC simulations, we repeated the Langevin equations with the same chaotic signal

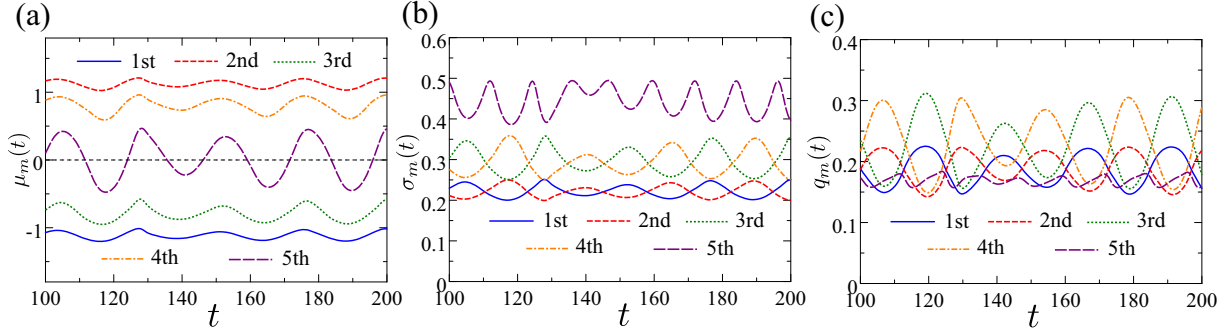


FIG. 7: (Color online) Time evolution of (a) the mean μ_m , (b) the standard deviation σ_m , and (c) the weight q_m , for each Gaussian basis ($N_B = 5$). In panels (a)–(c), the solid, dashed, dotted, dot-dashed, and long-dashed lines represent the quantities for the 1, 2, ..., 5th Gaussian bases, respectively. The parameters are $D = 0.2$, $\alpha = 0.02$ and $\omega = 0.25$.

10000 times to calculate the average. Along with results of VMGA with $N_B = 5$ plotted by solid lines, dot-dashed lines show those calculated by the VMGA with $N_B = 1$ which is similar to the MM case. In Figs. 6(a)–(c), we can see that the mean $\langle y(t) \rangle$ of the values obtained by the VMGA with $N_B = 5$ are in excellent agreement with that of the MC simulations, but not with that of the $N_B = 1$ model. The mean of the $N_B = 1$ values is located near 1 and it only approximates one of the two wells (the mean would be distributed around -1 for particular different initial values).

In order to study the properties of the VMGA in more detail, we considered the time evolution of the parameters of each of the Gaussian bases for $N_B = 5$. Figures 7(a), (b), and (c) show the mean μ_m , standard deviation σ_m , and weight q_m , respectively, of each Gaussian basis as a function of time t [μ_m , σ_m , and q_m were calculated by a_m , b_m , and r_m with Eqs. (A3)–(A5)]; the parameters were $D = 0.2$, $\alpha = 0.02$ and $\omega = 0.25$ identical to those used in Fig. 4(c). In Figs. 7(a)–(c), solid, dashed, dotted, dot-dashed, and long-dashed lines represent the quantities of the 1, 2, ..., 5th Gaussian bases, respectively. In Fig. 7(a), which shows the time evolution of the mean μ_m , we can see that the two wells are each approximated by two Gaussian distributions, and the temporal variation of the mean is at most ~ 1 (cf. 5th basis; long-dashed line). From the time evolution of the standard deviation σ_m [Fig. 7(b)], we see that the temporal variation as a function of time is small (about ~ 0.1), although the standard deviation averaged over time is different for each basis. In Fig. 7(c), all the weights q_m are distributed around 0.2, which shows that all of the bases

contributed to the PDF. As in the stationary case, the means of the various Gaussian bases do not follow the most probable path. Because the VMGA approximates the two wells with more than two Gaussian distributions, the mean properly approximates the exact time evolution.

Driven bistable systems subject to noise are often characterized by the maximal signal-to-noise ratio under adequate noise strength (SR). Although SR was originally studied in periodic signals, Ref. [23, 24] studied the SR effects in aperiodic signals. We quantified the extent of SR for aperiodic signals as follows:

$$C_0 = \frac{1}{T} \int_{t_0}^{t_0+T} \langle I(t)y(t + \mathcal{T}_0) \rangle dt = \frac{1}{T} \int_{t_0}^{t_0+T} I(t) \langle y(t + \mathcal{T}_0) \rangle dt, \quad (26)$$

where \mathcal{T}_0 is time lag yielding the maximal correlation:

$$\mathcal{T}_0 = \operatorname{argmax}_{\mathcal{T}} \frac{1}{T} \int_{t_0}^{t_0+T} I(t) \langle y(t + \mathcal{T}) \rangle dt. \quad (27)$$

Here, t_0 is the starting time and T is the duration of the observation; we again set $t_0 = 100$ and $T = 200$. C_0 evaluates the amount of chaotic information transmitted, and a larger value corresponds to better transmission. Although the SR for a chaotic signal was studied in view of noise-induced phase-synchronization [32, 34], the ASR obtained by calculating the correlation of Eq. (26) has not yet been studied. Figure 8 shows (a) the correlation C_0 , and (b) the time-lag \mathcal{T}_0 as a function the noise intensity D , where C_0 for the VMGA with $N_B = 5$ is shown by a solid line and that for the MC simulations is shown by circles. The parameters were $\alpha = 0.02$ and $\omega = 0.5$. C_0 achieves a maximum at $D \simeq 0.35$, which indicates the occurrence of ASR. Comparing the VMGA and MC results shown in Figs. 8(a) and (b), we see very good agreement, which verifies the reliability the VMGA. By using the VMGA, we can calculate properties of chaotically driven systems without performing stochastic simulations.

B. Chaotically driven bistable potential with colored noise

We next apply the VMGA to a bistable system with colored Gaussian noise. The one-dimensional colored Gaussian noise system can be embedded into a two-dimensional

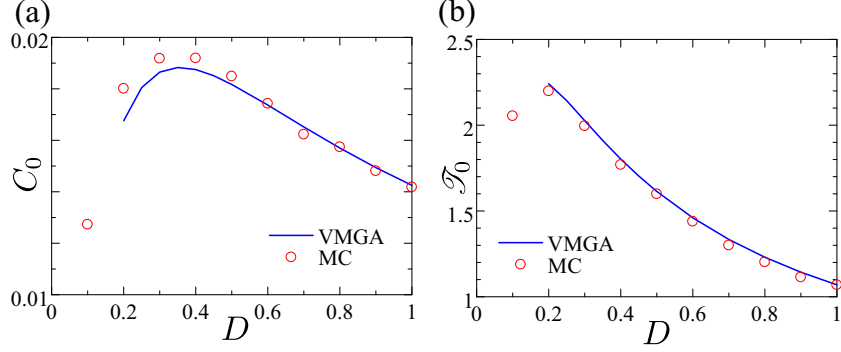


FIG. 8: (Color online) (a) Correlation C_0 [Eq. (26)], and (b) time-lag \mathcal{S}_0 [Eq. (27)] as a function of the noise intensity D , obtained by the VMGA with $N_B = 5$ (solid line) and by the MC simulations (circles). The parameters are $\alpha = 0.02$ and $\omega = 0.5$.

Langevin equation with white Gaussian noise:

$$\frac{dy}{dt} = y - y^3 + I(t) + z(t), \quad (28)$$

$$\frac{dz}{dt} = -\frac{z}{\tau} + \frac{\sqrt{D}}{\tau}\xi(t), \quad (29)$$

where $\xi(t)$ is white Gaussian noise [$\langle \xi(t)\xi(t') \rangle = 2\delta(t-t')$], $I(t)$ is the input signal, τ is the correlation time and $z(t)$ (the Ornstein–Uhlenbeck process) corresponds to a colored noise with the correlation $\langle z(t)z(t') \rangle = (D/\tau) \exp(-|t-t'|/\tau)$. We also employed the Rössler input for $I(t)$ [Eq. (22)]. The FPE operator $\hat{L}(y, z, t)$ of Eqs. (28)–(29) is

$$\hat{L}(y, z, t) = -\frac{\partial}{\partial y} (y - y^3 + z + I(t)) + \frac{1}{\tau} \frac{\partial}{\partial z} z + \frac{D}{\tau^2} \frac{\partial^2}{\partial z^2}. \quad (30)$$

Substituting Eq. (30) into Eq. (12), we can again calculate the K (the number of total parameters) coupled DAE with respect to $\boldsymbol{\theta} = (\mathbf{A}_m, \mathbf{b}_m, r_m)_{m=1}^{N_B}$ with

$$\mathbf{A}_m = \begin{pmatrix} a_{m,11} & a_{m,12} \\ a_{m,21} & a_{m,22} \end{pmatrix}, \quad \mathbf{b}_m = \begin{pmatrix} b_{m,1} \\ b_{m,2} \end{pmatrix}, \quad (31)$$

where $a_{m,12} = a_{m,21}$ (\mathbf{A}_m is a symmetric matrix). We require moments of up to the 6th order i.e., $\int_{-\infty}^{\infty} y^{n_y} z^{n_z} g(y, z; \mathbf{A}, \mathbf{b}) dy dz$ with $n_y + n_z \leq 6$, in order to obtain the DAE. As in the case with white Gaussian noise, Eq. (5) should be satisfied for the normalization, and the resulting $(K + 1)$ dimensional DAE is solved numerically.

Figures 9(a) and (b) show PDFs $P(y, z; t)$ at $t = 100$, which are calculated by MC simulations and the VMGA with $N_B = 5$, respectively, for $\tau = 0.1$ with $D = 1.0$, $\alpha = 0.02$

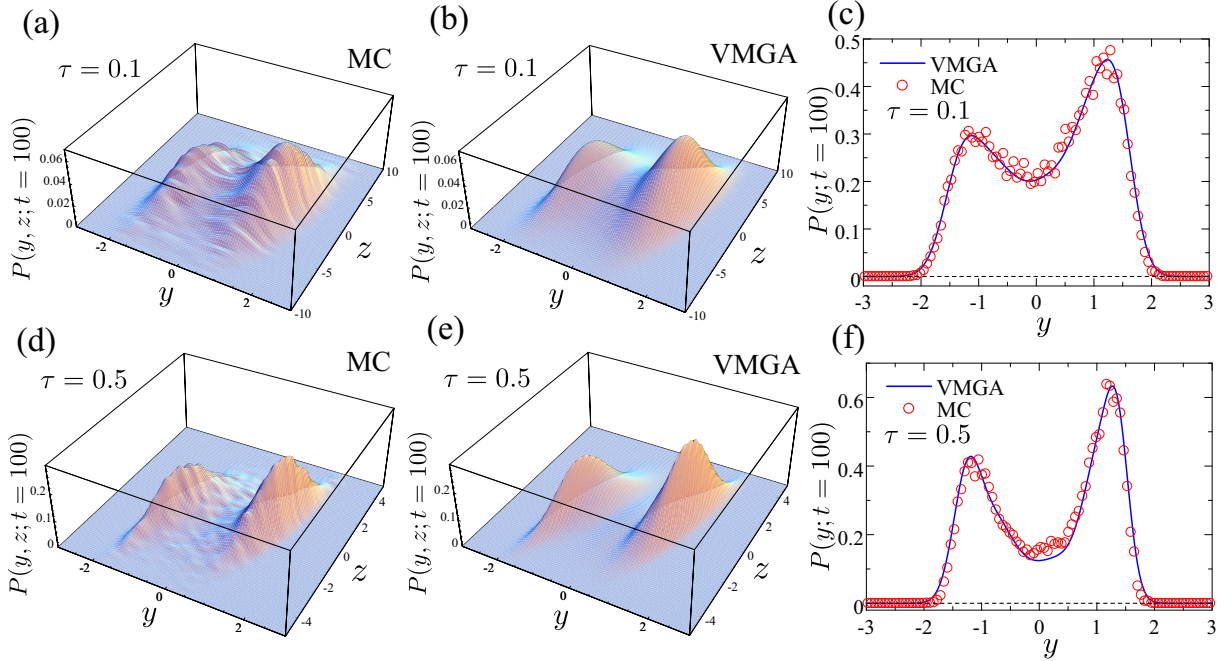


FIG. 9: (Color online) [(a), (b), (d), and (e)] PDFs $P(y, z; t)$ at time $t = 100$ for two τ settings [(a) and (b)] $\tau = 0.1$ and [(d) and (e)] $\tau = 0.5$ (other parameters are $D = 1.0$, $\alpha = 0.02$ and $\omega = 0.5$), where (a) and (d) are obtained by the MC simulations and (b) and (e) are obtained by the VMGA with $N_B = 5$. [(c) and (f)] Corresponding marginal PDFs $P(y; t)$ for (c) $\tau = 0.1$ and (f) $\tau = 0.5$; results of the VMGA and the MC simulations are shown by solid lines and circles, respectively.

and $\omega = 0.5$. To plot the results of the MC simulations as functions y and z , we employed kernel distributions. Figure 9(c) shows the marginal PDF $P(y; t) = \int_{-\infty}^{\infty} P(y, z; t) dz$, as calculated by MC simulations (circles) and by the VMGA with $N_B = 5$ (solid curve). Note that these are in good agreement. Figures 9(d) and (e) show similar PDFs $P(y, z; t)$, and Fig. 9(f) shows the marginal PDF $P(y; t)$ for $\tau = 0.5$ with $D = 1.0$, $\alpha = 0.02$ and $\omega = 0.5$. As in the one-dimensional case, the two Gaussian distributions approximate each of the single wells (and four Gaussian distributions approximate two wells), and the other well is at the center of the PDF. For $\tau = 0.5$, the peaks of the PDFs are steeper, and there is less agreement than in the $\tau = 0.1$ case between the PDFs $P(y, z; t)$ from the MC simulations and those from the VMGA. However, the marginal PDF $P(y; t)$ of the VMGA can accurately approximate the MC simulations. These results verify the reliability of the VMGA for the systems with colored Gaussian noise.

Next, we evaluated the dynamical properties of the VMGA by comparing the means $\langle y(t) \rangle$ of the MC simulations and the VMGA. Figure 10 shows the mean $\langle y(t) \rangle$ calculated by the MC simulation (dashed line) and from the VMGA with $N_B = 5$ (solid line), for two different parameters: (a) $\tau = 0.1$ and (b) $\tau = 0.5$; the other parameters were $D = 1.0$, $\alpha = 0.02$, and $\omega = 0.5$ (the parameters settings for Figs. 10(a) and (b) correspond to those in Figs. 9(a)–(c) and (d)–(f), respectively). In Figs. 10(a) and (b), the mean $\langle y(t) \rangle$ obtained from the VMGA is in good agreement with that of the MC simulations, for both τ values. As in the case with white Gaussian noise, the VMGA approximates the two wells with more than two Gaussian distributions, and hence the mean path obtained from the VMGA can accurately approximate the MC simulations. These results show that the VMGA can be applied to a two-dimensional system driven by external forces.

We also computed the correlation C_0 [Eq. (26)] of a chaotically driven system for the case with colored Gaussian noise. Figure 11(a) shows the correlation C_0 calculated by the VMGA with $N_B = 5$ as a function of the noise intensity D for two cases: $\tau = 0$ (i.e., the case of white noise, which is identical to that in Fig. 8; dashed line) and $\tau = 0.1$ (solid line) where other parameters are $\alpha = 0.02$ and $\omega = 0.5$. As seen in Fig. 11(a), C_0 also achieved the maximum value at an intermediate value of D (cf. the solid line). We see that the maximum value of C_0 for the white-noise case (dashed line) is smaller than that for colored-noise case (solid line) which indicates that the colored noise degrades the ASR effect. However, when the noise intensity is not optimal (i.e., $D > 0.6$), the colored noise can better transmit information. Figure 11(b) shows the time-lag \mathcal{T}_0 for the colored-noise case with $\tau = 0.1$ (solid line) and the white-noise case with $\tau = 0.0$ (dashed line). We note that the time lag for \mathcal{T}_0 with $\tau = 0.1$ is larger than that with $\tau = 0.0$; the time lag decreases as D increases, as in the case with white Gaussian noise.

IV. DISCUSSION AND CONCLUSION

The VMGA introduced in Section II can be used to obtain several time-dependent solutions of FPEs. We have shown that our approach can provide very accurate approximations by the superposition of multiple Gaussian distributions for one- and two-dimensional driven systems. We have modeled the mean, variance, and weight as time-dependent parameters. However, as inclusion of the covariance terms [\mathbf{A}_m in Eq. (13)] significantly increases the

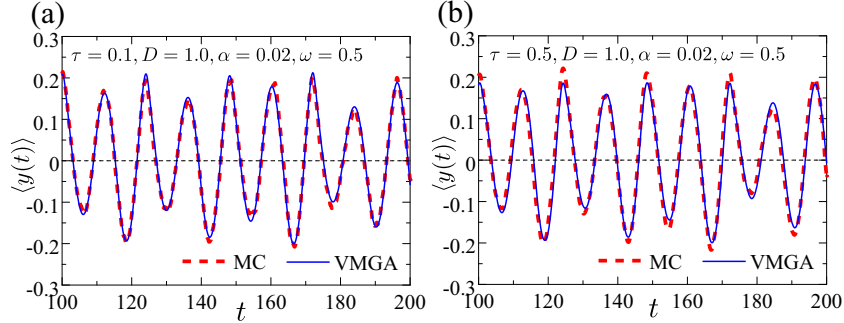


FIG. 10: (Color online) Time dependence of mean $\langle y(t) \rangle$ for (a) $\tau = 0.1$ and (b) $\tau = 0.5$, as calculated by MC simulations (dashed curve) and the VMGA with $N_B = 5$ (solid curve). The parameters are $D = 1.0$, $\alpha = 0.02$ and $\omega = 0.5$.

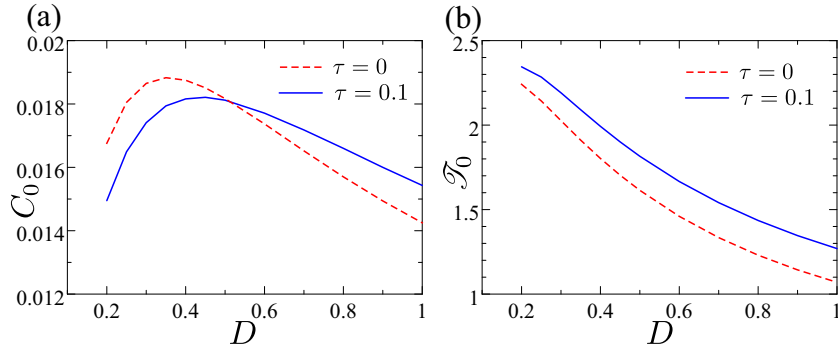


FIG. 11: (Color online) (a) Correlation C_0 [Eq. (26)] and (b) time lag \mathcal{T}_0 [Eq. (27)] calculated by the VMGA with $N_B = 5$, each as a function of the noise intensity D for $\tau = 0$ (white noise; solid line) and $\tau = 0.1$ (dashed line). The parameters are $\alpha = 0.02$ and $\omega = 0.5$.

number of parameters, taking the covariance as a constant is one possible approach to reducing the computational cost. This approach has been considered in the Gaussian wavepacket approximation in quantum mechanics [13] and is referred to as a *frozen* method (the time-dependent covariance model is called a *thawed* method). As shown in Fig. 7, the temporal variation of the standard deviation is around ~ 0.1 which is smaller than that of the mean. Therefore, if we can first specify the standard deviation of each Gaussian basis, we may ignore the time evolution of the variance. This frozen approximation could dramatically reduce the number of parameters in the VMGA where the parameter size K is

$$K = N_B(N + 1), \quad (32)$$

being linear with respect to the dimension N and smaller than that given by Eq. (15).

Although the effectiveness of the VMGA was demonstrated by our numerical results, it has some disadvantages. Because multiple Gaussian distributions are not orthogonal, the VMGA cannot calculate solutions when more than two Gaussian distributions coalesce. In theory, the accuracy of the VMGA increases when more basis functions are used. However, due to their nonorthogonality, an excessively large number of bases prevents the calculation of the time evolution of the parameters. Indeed, for the one-dimensional case, the VMGA could not calculate the time evolution with $N_B = 5$ for $D \lesssim 0.2$. For such cases, we should reduce N_B in order to enable the calculations. Similarly, for the two-dimensional case, colored noise with a larger time correlation tends to yield steeper peaks, which makes the application of the VMGA difficult with large N_B . Despite these disadvantages, however, the VMGA can provide a computationally efficient way to calculate the time-dependent dynamics of FPEs. Chaotically driven stochastic systems have often been solved by MC simulations. As shown in Section III, the VMGA successfully and very accurately calculated many of the quantities for the system without relying on stochastic approaches.

We applied the VMGA to a quartic bistable potential, where the moments of the Gaussian can be calculated in closed form. The integral in Eq. (12) can be computed analytically if the potentials are represented by polynomials. However, for general nonlinear models, the moment cannot necessarily be represented in closed form. In such situations, we may approximate the drift term $f_i(\mathbf{x})$ by the Taylor expansion:

$$f_i(\mathbf{x}) \simeq f_i(\boldsymbol{\mu}_g) + \nabla f_i(\boldsymbol{\mu}_g)^\top (\mathbf{x} - \boldsymbol{\mu}_g), \quad (33)$$

where $\boldsymbol{\mu}_g$ is the center of the Gaussian distribution in the integrand. Although we can handle arbitrary nonlinear models with Eq. (33), this approximation does not yield as reliable results as those presented in the present manuscript.

To summarize, we have proposed the VMGA for the time-dependent solution for Langevin equations by using the variational principle for superposition of multiple Gaussian distributions. Because we have shown the effectiveness of the VMGA in strongly nonlinear systems, we expect that the VMGA can be used to solve many real-world problems. Applications of the VMGA to other problems, such as to stochastic models of gene expression [2, 3], are left to our future study.

Appendix A: Relation to conventional multivariate Gaussian representation

The multivariate Gaussian distribution is generally given by the following representation:

$$\mathcal{N}(\mathbf{x}; \boldsymbol{\mu}, \boldsymbol{\Sigma}) = \frac{1}{(2\pi)^{n/2} \sqrt{|\boldsymbol{\Sigma}|}} \exp \left\{ -\frac{1}{2} (\mathbf{x} - \boldsymbol{\mu})^\top \boldsymbol{\Sigma}^{-1} (\mathbf{x} - \boldsymbol{\mu}) \right\}, \quad (\text{A1})$$

where $\boldsymbol{\mu}$ is the mean vector (column vector) and $\boldsymbol{\Sigma}$ is the covariance matrix (positive definite). In Eq. (A1), $|\boldsymbol{\Sigma}|$ denotes the determinant of $\boldsymbol{\Sigma}$. The mixture of multivariate Gaussian distributions is given by

$$P(\mathbf{x}; \{\boldsymbol{\mu}_m\}, \{\boldsymbol{\Sigma}_m\}, \{q_m\}) = \sum_{m=1}^{N_B} q_m \mathcal{N}(\mathbf{x}; \boldsymbol{\mu}_m, \boldsymbol{\Sigma}_m), \quad (\text{A2})$$

where q_m is the weight ($\sum_{m=1}^{N_B} q_m = 1$). This conventional representation and Eq. (13) are related in the following way:

$$\mathbf{A}_m = \frac{\boldsymbol{\Sigma}_m^{-1}}{2}, \quad (\text{A3})$$

$$\mathbf{b}_m = \boldsymbol{\Sigma}_m^{-1} \boldsymbol{\mu}_m, \quad (\text{A4})$$

$$r_m = \frac{q_m}{(2\pi)^{n/2} \sqrt{|\boldsymbol{\Sigma}_m|}} \exp \left\{ -\frac{1}{2} \boldsymbol{\mu}_m^\top \boldsymbol{\Sigma}_m^{-1} \boldsymbol{\mu}_m \right\}. \quad (\text{A5})$$

According to Eq. (A3), \mathbf{A}_m is positive definite since it is the inverse of a positive definite matrix ($\boldsymbol{\Sigma}$ is positive definite). The inverse transform of Eqs. (A3)–(A5) is

$$\boldsymbol{\Sigma}_m = \frac{1}{2} \mathbf{A}_m^{-1}, \quad (\text{A6})$$

$$\boldsymbol{\mu}_m = \frac{1}{2} \mathbf{A}_m^{-1} \mathbf{b}_m, \quad (\text{A7})$$

$$q_m = \frac{r_m \pi^{n/2}}{\sqrt{|\mathbf{A}_m|}} \exp \left\{ \frac{1}{4} \mathbf{b}_m^\top \mathbf{A}_m^{-1} \mathbf{b}_m \right\}. \quad (\text{A8})$$

In Eqs. (A3)–(A8), we used the fact that \mathbf{A}_m is symmetric.

Appendix B: Initial values of DAE

One of the difficulties in our approach is to find valid initial values for the DAEs. Unlike conventional (explicit) ordinary differential equations, DAEs must satisfy an equality condition, and some parameters should be determined numerically by that equality (in our implementation, this was done automatically by *MATHEMATICA* 10). We found that calculating the equality is difficult in some cases. For larger noise intensities D (for both the

white- and colored-noise cases) and for smaller correlation times τ (for the colored-noise case), it is relatively easy to find valid initial values for the DAE. Therefore, when finding initial values when D is smaller, we first find valid initial values with $D = 1.0$ (large D value) and then iterate the calculations, adopting the converged stationary values of the preceding D values as the initial values used to find the next D value. It is also possible to adjust the system by making D (or τ) a time-dependent parameter and assuming that D (τ) decreases (increases) over time starting from large D (small τ) value. This time-dependent technique was employed for the $\tau = 0.5$ case.

Acknowledgment

This work was supported by a Grant-in-Aid for Young Scientists B (Y.H.: No. 25870171) from Ministry of Education, Culture, Sports, Science, and Technology (MEXT), Japan.

-
- [1] V. Kampen, *Stochastic Process Theory in Physics and Chemistry* (North-Holland, 1992).
 - [2] Y. Hasegawa and M. Arita, *J. R. Soc. Interface* **11**, 20131018 (2014).
 - [3] Y. Hasegawa and M. Arita, *Phys. Rev. Lett.* **113**, 108101 (2014).
 - [4] F. Ritort, in *Advances in Chemical Physics*, edited by S. A. Rice (Wiley publications, 2008), vol. 137, pp. 31–123.
 - [5] U. Seifert, *Rep. Prog. Phys.* **75**, 126001 (2012).
 - [6] H. Huang and N. M. Ghoniem, *Phys. Rev. E* **51**, 5251 (1995).
 - [7] R. Rodriguez and H. C. Tuckwell, *Phys. Rev. E* **54**, 5585 (1996).
 - [8] H. C. Tuckwell and J. Jost, *Physica A* **388**, 4115 (2009).
 - [9] A. D. McLachlan, *Mol. Phys.* **8**, 39 (1964).
 - [10] P. A. M. Dirac, *Math. Proc. Camb. Phil. Soc.* **26**, 376 (1930).
 - [11] J. Frenkel, *Wave Mechanics, Advanced General Theory* (Oxford: Clarendon Press, 1934).
 - [12] J. Broeckhove, L. Lathouwers, E. Kesteloot, and P. Van Leuven, *Chem. Phys. Lett.* **149**, 547 (1988).
 - [13] R. T. Skodje and D. G. Truhlar, *J. Chem. Phys.* **80**, 3123 (1984).
 - [14] G. A. Worth, M. A. Robb, and I. Burghardt, *Farad. Discuss.* **127**, 307 (2004).

- [15] J. O. Zoppe, M. L. Parkinson, and M. Messina, *Chem. Phys. Lett.* **407**, 308 (2005).
- [16] G. Terejanu, P. Singla, T. Singh, and P. D. Scott, *J. Guid. Control Dynam.* **31**, 1623 (2008).
- [17] H. Risken, *The Fokker–Planck Equation: Methods of Solution and Applications* (Springer, 1989), 2nd ed.
- [18] G. W. Harrison, *Numer. Meth. Part. D. E.* **4**, 219 (1988).
- [19] P. Kumar and S. Narayanan, *Sadhana* **31**, 445 (2006).
- [20] J. C. Whitney, *J. Comput. Phys.* **6**, 483 (1970).
- [21] T. Wilhelm, *BMC Syst. Biol.* **3**, 90 (2009).
- [22] P. Jung, *Phys. Rep.* **234**, 175 (1993).
- [23] J. J. Collins, C. C. Chow, and T. T. Imhoff, *Phys. Rev. E* **52**, R3321 (1995).
- [24] J. J. Collins, C. C. Chow, A. C. Capela, and T. T. Imhoff, *Phys. Rev. E* **54**, 5575 (1996).
- [25] R. Benzi, A. Sutera, and A. Vulpiani, *J. Phys. A* **14**, L453 (1981).
- [26] B. McNamara and K. Wiesenfeld, *Phys. Rev. A* **39**, 4854 (1989).
- [27] L. Gammaitoni, P. Hänggi, P. Jung, and F. Marchesoni, *Rev. Mod. Phys.* **70**, 223 (1998).
- [28] M. D. McDonnell, N. G. Stocks, C. E. M. Pearce, and D. Abbott, *Stochastic resonance* (Cambridge University Press, 2008).
- [29] M. D. McDonnell and D. Abbott, *PLoS Comput. Biol.* **5**, e1000348 (2009).
- [30] U. M. Ascher and L. R. Petzold, *Computer methods for ordinary differential equations and differential-algebraic equations* (Siam, 1998).
- [31] O. E. Rössler, *Phys. Lett. A* **57**, 397 (1976).
- [32] A. Silchenko, T. Kapitaniak, and V. Anishchenko, *Phys. Rev. E* **59**, 1593 (1999).
- [33] G.-K. Er, *Int. J. Non-Linear Mechanics* **33**, 201 (1998).
- [34] C. Eichwald and J. Walleczek, *Phys. Rev. E* **55**, R6315 (1997).